Global distribution of CT2 at altitudes 30–50 km from space-borne observations of stellar scintillation

Alexandre S. Gurvich, Viktoria F. Sofieva, Francis Dalaudier

Global distribution of C_T^2 at altitudes 30–50 km from space-borne observations of stellar scintillation

A. S. Gurvich,[1] V. F. Sofieva,[2] and F. Dalaudier[3]

Received 26 June 2007; revised 14 September 2007; accepted 12 November 2007; published 28 December 2007.

[1] Locally isotropic turbulence in the stratosphere consists of isolated sporadic patches with random values of temperature structure characteristic C_T^2. Stellar scintillations measured aboard GOMOS/ENVISAT through the Earth atmosphere provided the first global distribution of the effective characteristic $C_{T,eff}^2$ averaged along sounding ray. For zonal mean, the largest values are achieved in winter polar regions. This observed intense turbulence is probably related to the polar night jet. Relatively weak turbulence is observed at low latitudes. Turbulence intensity map is shown for altitude 42 km in the latitude band ±35°, where the maxima follow the sub-solar latitude, with enhancements located mainly over continents. Turbulence enhancements are not related with orography. Despite a noticeable correlation with typical regions of deep convection, the overall distribution of $C_{T,eff}^2$ displays a more complicated structure. Analyzed data suggest that the main turbulence sources, at altitudes ~40 km, are instabilities of stratospheric circulation and gravity wave breaking. **Citation:** Gurvich, A. S., V. F. Sofieva, and F. Dalaudier (2007), Global distribution of C_T^2 at altitudes 30–50 km from space-borne observations of stellar scintillation, *Geophys. Res. Lett.*, *34*, L24813, doi:10.1029/2007GL031134.

1. Introduction

[2] Breaking of internal gravity waves (IGW) and instabilities of different kind (e.g., shear instability, convective instability etc.) generate turbulence in the stratosphere. Turbulence constitutes the last stage of kinetic energy dissipation into heat through molecular diffusion. *Phillips* [1967] has shown that turbulence in the stable stratosphere consists of isolated sporadic patches. These patches seem to take the form of "pancakes" whose horizontal length scale is much larger than the vertical one. Radar returns visualize these patches [*Atlas*, 1965]. Because of flatness of turbulent patches, they appear as turbulent layers in balloon soundings [*Coulman et al.*, 1995]. Nowadays, there are no systematic observational data of turbulence at altitudes 30–50 km. These altitudes are not accessible for airplane exploration. Routine radiosondes usually reach a little higher than 30 km. Rocket soundings [*Lübken*, 1997] usually give information about the atmosphere above 60 km. Radio occultation technique provides reliable data below 30 km [*Gorbunov*, 2002]. Radar returns cannot usually be observed for altitudes 30–50 km.

[3] Information about air density irregularities for these altitudes are available from lidar studies [*Wilson et al.*, 1991; *Whiteway and Carswell*, 1995; *Sica and Russell*, 1999]. However, lidar data are rare and they are bounded to a specific location. Air temperature irregularities with vertical scales larger than few kilometres are studied by using observations of infrared [*Eckermann and Preusse*, 1999] and microwave [*Wu and Waters*, 1996] emissions.

[4] Using satellite measurements of stellar scintillation is an alternative approach that allows remote sensing of small-scale processes, with scales down to fractions of meter, in the stratosphere [*Gurvich*, 2002]. This approach is based on the theory of scintillations developed by *Tatarskii* [1971]. It connects scintillation spectra with spectra of air density irregularities. Waves and turbulence create irregularities of air refractivity δn, which are proportional to fluctuations of air density $\delta\rho$. When a star is observed on board a satellite, stellar flux passed through the atmosphere exhibits scintillation caused by these fluctuations. Analyses of scintillation measurements on board the MIR station allowed the retrieval of parameters of IGW and turbulence spectra [*Gurvich and Kan*, 2003a, 2003b]. However, the man-controlled photometer on board MIR allowed only a small number of observations in the latitude band ±60°. The scintillation measurements became available with global coverage since the launch of Envisat satellite in 2002. The GOMOS (Global Ozone Monitoring by Occultation of Stars) instrument on board ENVISAT is equipped with two fast photometers (FP) operating at blue (470–520 nm) and red (650–700 nm) wavelengths λ with the sampling frequency f_s = 1 kHz (http://envisat.esa.int/instruments/gomos). Analysis of coherency spectra of the GOMOS scintillation data [*Gurvich et al.*, 2005] has shown the presence of stratospheric layers with large intensity of isotropic turbulence. The analysis of scintillation variance for two seasons of year 2003 is presented by *Sofieva et al.* [2007a].

[5] In this paper, we present the first global and seasonal distribution of the structure characteristic C_T^2 of isotropic turbulence at altitudes 30–50 km obtained from scintillation measurements by GOMOS FP in 2003.

2. Model and Processing

[6] Observed scintillation is the result of light waves diffraction on refractivity irregularities δn that are proportional to irregularities of air density [*Tatarskii*, 1971]. The main contribution to energy of turbulent scintillations comes from irregularities of light field with scales smaller than a few tens of meters [*Gurvich and Kan*, 2003a, 2003b]. The scintillations caused by IGW have larger scales and can be separated from small-scale turbulent scintillation by spectral analysis. Ignoring turbulent fluctuations of pressure, turbu-

[1] A. M. Oboukhov Institute of Atmospheric Physics, Moscow, Russia.
[2] Earth Observation, Finnish Meteorological Institute, Helsinki, Finland.
[3] Service d'Aeronomie du CNRS, Verrières-le-Buisson, France.

0094-8276/07/2007GL031134

lent irregularities δn are connected with temperature irregularities δT: $\delta n = -(\langle n\rangle/\langle T\rangle)\delta T$, where $\langle n\rangle$ and $\langle T\rangle$ are the mean refractivity and temperature at a given altitude. Propagation of light waves through the stratosphere containing turbulent patches can be considered as propagation through a random media with variable parameters.

[7] Let us assume that temperature irregularities in turbulent patches have the Kolmogorov's 3D spectrum: $\Phi_T(\kappa) = 0.033\, C_T^2 \kappa^{-11/3} \exp(-\kappa^2/\kappa_m^2)$, with parameters: C_T^2, the structure characteristic, and κ_m, the wave number corresponding to the inner scale. We assume that sizes of turbulent patches are random, as well as parameters C_T^2 and κ_m in them. Hence 3D spectrum of δn in a patch is

$$\Phi_n(\kappa) = 0.033\langle n\rangle^2\langle T\rangle^{-2} C_T^2 \kappa^{-11/3} \exp\left(-\kappa^2/\kappa_m^2\right). \quad (1)$$

Mean refractivity $\langle n(h)\rangle$ decreases almost exponentially with altitude h, with the atmospheric scale height $H_0(h)$. Therefore the region of main interaction between light waves and δn is located around the perigee of a sounding ray. Horizontal size L_A of this region is a few hundreds of kilometers; the ray can cross many patches. Satellite observations are performed at a large distance L ($L \gg L_A$) from the ray perigee. For GOMOS, L = 3200 km. Integrating 2D scintillation spectra [*Tatarskii*, 1971, equations (4.48) and (5.48)], we calculate the variance σ_I^2 of isotropic scintillation in the observation plane:

$$\begin{aligned}
\sigma_I^2 &= \frac{2.25}{\cos(5\pi/12)} k_0^{7/6} L^{5/6} \int_{\text{ray}} dx C_n^2(x) W^{-5/3} \\
&\quad \cdot \left[\left(1+W^4\right)^{5/12} \cos\left(5\text{atan}\left(W^2\right)/6\right) - 1\right], \\
C_n^2(x) &= \frac{\langle n(h_0)\rangle^2}{\langle T(h_0)\rangle^2} \exp\left(-\frac{x^2}{R_E H_0}\right) C_T^2(x), \\
W &= \kappa_m(x)\sqrt{L/k_0},\ k_0 = \frac{2\pi}{\lambda}
\end{aligned} \quad (2)$$

where x is the coordinate along ray, $x = 0$ and $x = L$ correspond to the ray perigee point and to the observation plane, respectively, R_E is the Earth radius. Turbulent fluctuations of temperature significantly exceed that of pressure $\delta T/\langle T\rangle \gg \delta P/\langle p\rangle$; this is taken into account in (2).

[8] If the inner scale of turbulence κ_m^{-1} is much smaller than Fresnel scale $Fr = \sqrt{L/k_0}$ (equivalently $W \gg 1$), Equation (2) can be transformed to:

$$\begin{aligned}
\sigma_I^2 &= 2.25 k_0^{7/6} L^{5/6} L_A \frac{\langle n(h_0)\rangle^2}{\langle T(h_0)\rangle^2} C_{T,\text{eff}}^2, \\
C_{T,\text{eff}}^2 &= L_A^{-1} \int_{-\infty}^{\infty} dx \exp\left(-\frac{x^2}{R_E H_0}\right) C_T^2(x)
\end{aligned} \quad (3)$$

The parameter $C_{T,\text{eff}}^2$ is C_T^2 averaged along a ray with the weight function $L_A^{-1} \exp(-x^2/R_E H_0)$ determining the effective region of interaction between the light wave and the turbulent atmosphere. Its horizontal size is $L_A = \sqrt{\pi R_E H_0}$.

[9] Equations (2) and (3) give an opportunity for estimating $C_{T,\text{eff}}^2$ from space-borne observations of stellar scintillation. However, modest sampling frequency of GOMOS photometers does not allow estimating κ_m from the scintillation data, thus real values of W are uncertain. Previous space-born observations of stellar scintillation [*Gurvich and Kan*, 2003b] have shown that values of $1/\kappa_m$ do not exceed 0.6 m at altitudes 30 ÷ 50 km, the mean of $1/\kappa_m$ is ~ 0.2 ÷ 0.3 m. Since $\sqrt{L/k_0}$ = 0.59 m for the red FP, we can assume $W > 1$ along the ray. The influence of the parameter W on σ_I^2 in equation (2) is described by a smooth monotonous function $g(W) = \cos^{-1}(5\pi/12) W^{-5/3}[(1 + W^4)^{5/12} \cos(5\text{atan}(W^2)/6) - 1]$, $g(\infty) = 1$, $g(1) = 0.228$. According to the mean-value theorem, the use of a constant value $g(W_{\text{eff}}) = 0.7$, which corresponds to the effective value of $1/\kappa_m$ = 0.21 m, introduces an uncertainty less than 50% in the resulting σ_I^2.

[10] Scintillations are recorded along a spacecraft trajectory with the integration time $\tau_S = f_S^{-1}$. The scale of time averaging is $\tau_S u$ (u is the projection of the satellite velocity on the observation plane), while the typical scintillation scale on the observation plane is max ($1/\kappa_m$, Fr) [*Tatarskii*, 1971]. In GOMOS observations $\tau_S u > \max(1/\kappa_m, Fr)$, thus the variance of recorded isotropic scintillation β_{iso}^2 is smaller than σ_I^2 defined by (2) by a factor G. The effect of temporal smoothing is estimated by using the above cited equations (4.48) and (5.48) from *Tatarskii* [1971] and assuming $C_T^2(x) = C_{T,\text{eff}}^2$ and $W = W_{\text{eff}} = const$. This results in the approximation $G = 1.63\ [(u\tau)^2\ k_0/L]^{-0.485}\ [g(W_{\text{eff}})]^{-0.39}$. The accuracy of this approximation is better than 1 ÷ 2 % for possible values of turbulence parameters, 3.4 km/s < u < 6.5 km/s and $W_{\text{eff}} > 1$. Finally, we obtain β_{iso}^2:

$$\begin{aligned}
\beta_{\text{iso}}^2 &= 2.25 k_0^{7/6} L^{5/6} L_A \langle n(h_0)\rangle^2 \langle T(h_0)\rangle^{-2} \\
&\quad \cdot G\left(u\tau/\sqrt{L/k_0}, W_{\text{eff}}\right) g(W_{\text{eff}}) C_{T,\text{eff}}^2
\end{aligned} \quad (4)$$

The above equations are derived for monochromatic radiation and without refractive dilution. The impact of refractive dilution and averaging over wavelength band of the FP optical filter [*Dalaudier et al.*, 2001] are not significant at altitudes above 30 km compared to uncertainty of κ_m discussed above. The equation (4) is the base for determination of C_T^2 from space-borne observations of stellar scintillation. We leave out the subscript "eff" hereafter for short. The above results are based on the theory of weak scintillations i.e. when $\sigma_I^2 < 1$. In case of strong scintillation, it is very difficult to separate scintillations caused by turbulence and IGW. In our analysis, we consider the altitude range above 30 km, where the weak scintillation assumption is valid [*Gurvich and Kan*, 2003a].

[11] β_{iso}^2 can be determined from GOMOS scintillations by using the technique described in detail by *Sofieva et al.* [2007a]. This technique uses the fact that scintillation spectra at wave numbers larger than the inverse of IGW's inner scale are defined mainly by the turbulent component. The scintillation spectrum of the turbulent component is nearly flat in the wave number range available from GOMOS measurements [*Tatarskii*, 1971; *Sofieva et al.*, 2007b]. This allows separating the IGW and turbulent contributions from the observed scintillation variance and thus computing β_{iso}^2 (for details and illustration of this method, see *Sofieva et al.* [2007a, section 2 and Figure 3]). Known β_{iso}^2, C_T^2 is determined using (4).

3. Results and Discussion

[12] Locations of dark-limb occultations of 30 brightest stars in 2003 selected for analysis are shown in Figure 1.

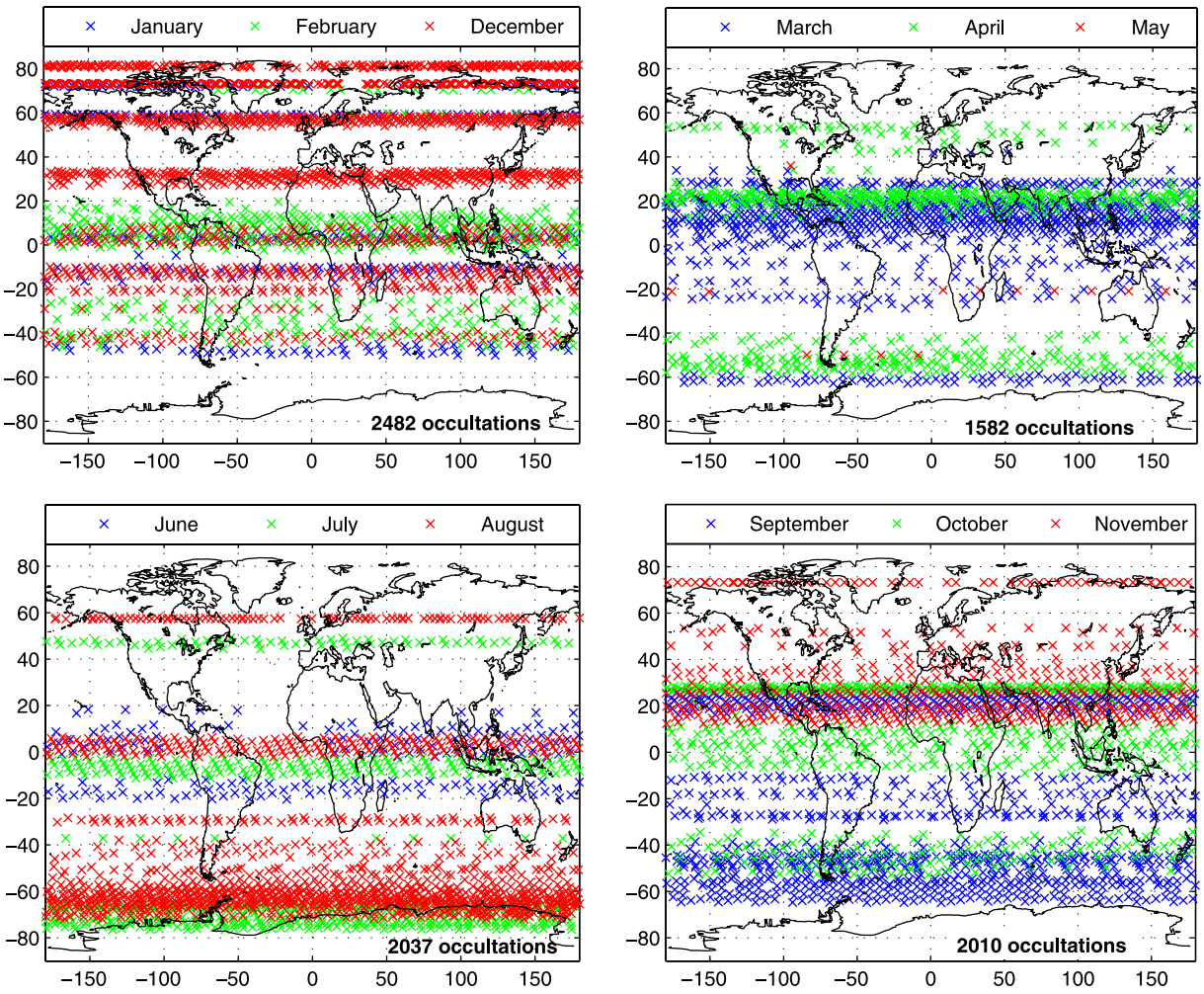

Figure 1. Location of the selected occultations in four seasons of year 2003.

The observed structure of latitude bands is the consequence of the non-uniform distribution of the brightest stars. The red photometer measurements are used for C_T^2 computation, as they are less affected by absorption and scattering in the atmosphere. The profiles of C_T^2 are computed for each individual occultation. The coverage by bright stars is not sufficient for obtaining monthly global maps (as can be seen in Figure 1), therefore we restricted ourselves by considering seasonal distributions. For producing plots of zonal mean C_T^2, the data are averaged in latitudinal bins distributed in accordance with available data: the centers of the bins are assigned to the characteristic latitudes corresponding to occultation series. The width of latitudinal bins is mostly $\sim 10°$, but it ranges from 5° to 30°. The median values of C_T^2 at each altitude are used for the construction of Figure 2 due to robust properties of the median estimates of highly variable dataset.

[13] Figure 2 shows the distribution of zonal median C_T^2 in four seasons of 2003 obtained from observations indicated in Figure 1. First of all, large variations of C_T^2 can be noticed: the range of possible values of C_T^2 covers more than two orders of magnitude, from 3×10^{-5} to 6×10^{-3} $K^2 m^{-2/3}$. The value of C_T^2 has a clear physical sense. It equals to the variance of the temperature difference in two points at the distance of one meter. The largest C_T^2 values are observed in the boundary layer [*Tatarskii*, 1971], where values of C_T^2 vary depending on insolation, wind velocity, underlying surface and so on. Values of C_T^2 usually decrease with altitude in the troposphere [*Gavrilov et al.*, 2005; *Zink et al.*, 2004]. Typical values for the lower stratosphere (below 30 km) may cover more than two orders of magnitude. Above 30 km and up to 70 km, there exists scanty data obtained from spacecraft scintillation observations [*Gurvich and Kan*, 2003a, 2003b]. They show the definite increase of C_T^2 with altitude from some units of 10^{-4} to some units 10^{-3}, with scattering about one order of magnitude at $30 \div 50$ km, for different locations and observation time. In the mesosphere, *Lübken* [1992] reported the values of the structure characteristic of relative refractivity fluctuations C_n^2 at altitudes 84–85 km, as obtained from rocket soundings. The corresponding C_T^2 values are $\sim 10^{-1}$ K^2 $m^{-2/3}$.

[14] Values of C_T^2 shown in Figure 2 are within the range of the values given by *Gavrilov et al.* [2005], *Zink et al.* [2004], and *Lübken* [1992, 1997]. Wide range of C_T^2 variation explains the data scattering of *Gurvich and Kan* [2003a, 2003b]. The maps for Jan–Feb–Dec and Jun–Jul–Aug are almost mirror-symmetric. The largest values of C_T^2 are observed above $40 \div 45$ km in polar winter in both hemispheres; they are especially large in the Southern Hemisphere. The strong turbulence here is probably related

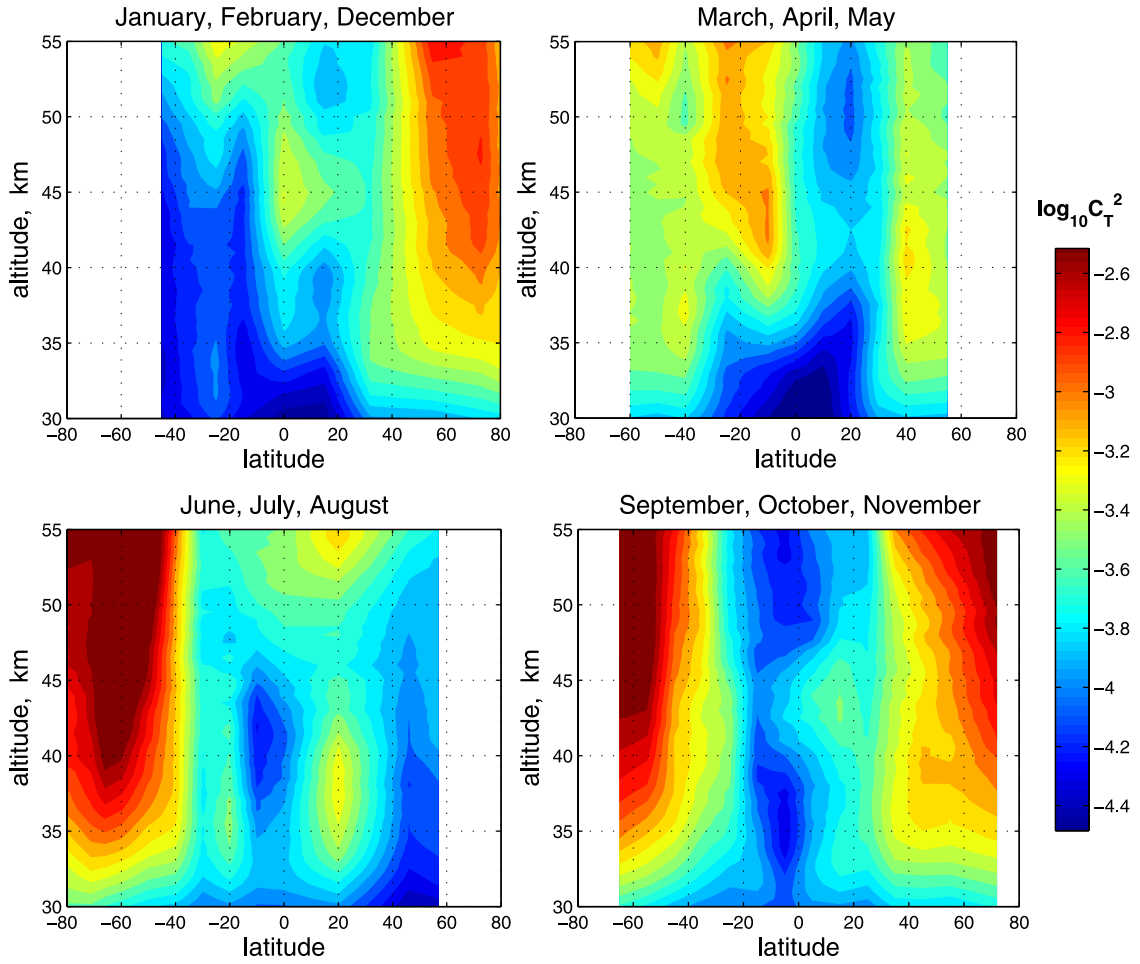

Figure 2. Zonal averaged C_T^2(K^2 m$^{-2/3}$) in four seasons of 2003, logarithmic color scale.

to the polar night jet [*Holton*, 2004]. Based on the simplified spectral analysis, *Sofieva et al.* [2007a] suggested that the strong turbulence at winter polar stratosphere might be related with breaking IGW in the polar night jet. Several previous observational studies [*Duck et al.*, 1998, 2001; *Jiang and Wu*, 2001] also pointed out that the gravity waves should break in the polar night jet at altitudes close to stratopause, in order to explain the thermal balance in the polar vortex area. Local enhancement of turbulence at the edge of the polar vortex during the sudden stratospheric warming in December 2003 (which also contributes to the distribution shown in Figure 2) is discussed by *Sofieva et al.* [2007b]. The plot for Sep–Oct–Nov shows enhancements at high latitudes, in both hemispheres. However, taking into account that in SH the measurements were carried out mainly in September, while in NH they were performed in November (Figure 1), these enhancements are most probably related to the remaining (beginning) of the polar vortex. This is confirmed, in particular, by the distribution of C_T^2 in Mar–Apr–May. The major part of occultations were carried out in April, and the distribution of C_T^2 has smaller variations. In addition to the noted peculiarities at polar latitudes, modest enhancements in zonal mean turbulence around 20°S in March–May and some smaller ones around 20°N in June–August are observed.

[15] Figure 3 shows the geographical distribution of C_T^2 in the layer about 3 km thick (vertical resolution) centered at altitude ~42 km, between 35N and 35S. We selected this altitude, because the previous consideration of GOMOS scintillation data [*Gurvich et al.*, 2005] has shown that turbulence is observed more clearly on the IGW background at these altitudes. Turbulence intensity is smaller in this zone than in polar regions and, in average, it has a pronounced zonal structure. The plots of Figure 3 show that the average values of C_T^2 follow the sub-solar latitude like main distinctive feature of general circulation of the middle atmosphere [*Holton*, 2004]. At the same time, almost all of the local enhancements are over continents (except for that one over Western Pacific in June–September). Many of C_T^2 enhancements seen in Figure 3 correspond well to the typical regions of deep convection, e.g., Africa, South America and Indonesia in Dec, Jan–March, regions of Indian and American monsoons and of North African dry convection in June–September [*Jiang et al.*, 2004]. Many similarities can be found between enhancements in C_T^2 shown in Figure 3 and local maxima of temperature variances at ~38 km obtained from MLS data [*Jiang et al.*, 2004, Figure 4]. In spite of the large difference in spatial scales (many hundreds times), it is possible to assume that the observed enhancements in C_T^2 correspond to the last step (before molecular diffusion) of breakdown of temperature

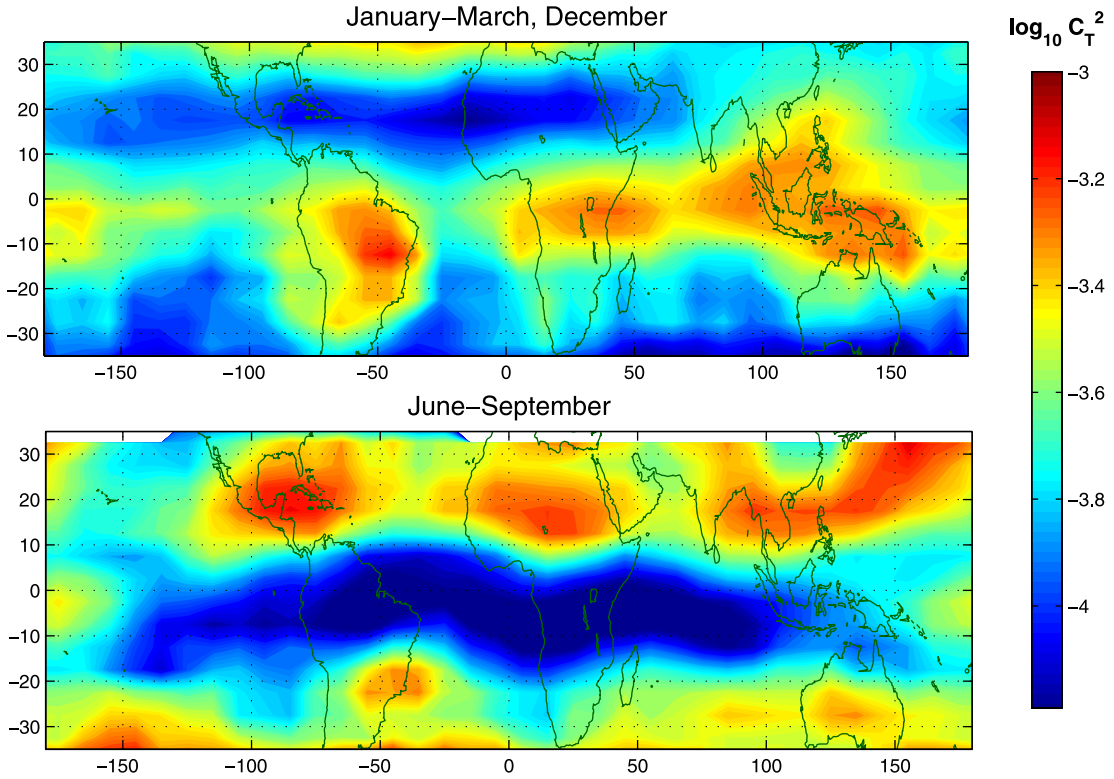

Figure 3. C_T^2(K^2 m$^{-2/3}$) at 42 km for (top) Jan–March, Dec. and for (bottom) June–Sept., logarithmic color scale. The data are averaged in 5° × 10° latitude-longitude bins and a three-point smoothing is applied to the obtained fields. In order to make these maps more contrasting, the color scale covers one decade only.

irregularities observed by MLS and interpreted as IGW. However, this question requires a deeper analysis and is beyond the scope of this paper.

[16] Turbulence in the stratosphere results not only from IGW breaking but also from different kind of instabilities [*Staquet and Sommeria*, 2002], therefore the distribution of C_T^2 has a more complicated structure: some of local maxima of C_T^2 (e.g. over Western Brazil and over Australia in Jun–Sep) do not correspond either to typical regions of convection or to mountain GW.

[17] No systematic increase of C_T^2 over large mountain range such as Himalaya, Andes and Sierra Nevada is observed in seasonal average distributions shown in Figure 3. Probably mountain waves are too long for transformation into small scale turbulence observed by scintillation at 42 km.

4. Summary

[18] Analysis of GOMOS stellar scintillation observations gave the first estimation of global distribution of C_T^2 at altitudes 30–50 km for four seasons. The values of zonal mean C_T^2 increase with the altitude, as a rule. The largest C_T^2 values are achieved in polar regions in winter, where they may reach 0.006 K^{2}m$^{-2/3}$ in SH, i.e. the values, which are comparable with those observed in the turbulent boundary layer. It can be assumed that this observed intense turbulence is related to the polar night jet.

[19] Relatively low turbulence is observed at low latitudes. Minimal values of C_T^2 are less than 10^{-4} K^{2}m$^{-2/3}$ there. The average turbulence intensity at altitudes ~42 km follows the solstice, with enhancements located mainly over continents. Turbulence enhancements in tropical regions are not related with orography. Despite a good correlation with typical regions of deep convection, the overall distribution of C_T^2 displays a more complicated structure. These peculiarities of C_T^2 fields and the observed zonal structure in turbulence distribution indicate that the main turbulence sources are instabilities of general stratospheric circulation of different kind and IGW breaking induced by these instabilities.

[20] **Acknowledgments.** The authors thank ESA, ACRI-ST and the GOMOS team for the GOMOS data. The work of AG was supported by RFBR grant 06-05-64357. The work of VS was supported by the Academy of Finland.

References

Atlas, D. (1965), Angels in focus, *J. Res. Natl. Bur. Stand., Sect. D*, *69*, 871–875.

Coulman, C. E., J. Vernin, and A. Fuchs (1995), Optical seeing—Mechanism of formation of thin turbulent laminae in the atmosphere, *Appl. Opt.*, *34*, 5461–5474.

Dalaudier, F., V. Kan, and A. S. Gurvich (2001), Chromatic refraction with global ozone monitoring by occultations of stars. I. Description and scintillation correction, *Appl. Opt.*, *40*, 866–877.

Duck, T. J., J. A. Whiteway, and A. I. Carswell (1998), Lidar observations of gravity wave activity and Arctic stratospheric vortex core warming, *Geophys. Res. Lett.*, *25*(15), 2813–2816.

Duck, T. J., J. A. Whiteway, and A. I. Carswell (2001), The gravity wave-Arctic stratospheric vortex interaction, *J. Atmos. Sci.*, *58*, 3581–3596.

Eckermann, S. D., and P. Preusse (1999), Global measurements of stratospheric mountain waves from space, *Science*, *286*, 1534–1537.

Gavrilov, N. M., H. Luce, M. Crochet, F. Dalaudier, and S. Fukao (2005), Turbulence parameter estimations from high-resolution balloon temperature measurements of the MUTSI-2000 campaign, *Ann. Geophys.*, *23*, 2401–2413.

Gorbunov, M. E. (2002), Ionospheric correction and statistical optimization of radio occultation data, *Radio Sci.*, *37*(5), 1084, doi:10.1029/2000RS002370.

Gurvich, A. S. (2002), Parameters of turbulence and internal waves and the dissipation of kinetic energy in the stratosphere based on space observations, *Dokl. Earth Sci.*, *385*(5), 599–603.

Gurvich, A. S., and V. Kan (2003a), Structure of air density irregularities in the stratosphere from spacecraft observations of stellar scintillation, 1. Three-dimensional spectrum model and recovery of its parameters, *Izv. Russ. Acad. Sci. Atmos. Oceanic Phys.*, *39*, 300–310.

Gurvich, A. S., and V. Kan (2003b), Structure of air density irregularities in the stratosphere from spacecraft observations of stellar scintillation, 2. Characteristic scales, structure characteristics, and kinetic energy dissipation, *Izv. Russ. Acad. Sci. Atmos. Oceanic Phys.*, *39*, 311–321.

Gurvich, A. S., F. Dalaudier, and V. F. Sofieva (2005), Study of stratospheric air density irregularities based on two-wavelength observation of stellar scintillation by Global Ozone Monitoring by Occultation of Stars (GOMOS) on Envisat, *J. Geophys. Res.*, *110*, D11110, doi:10.1029/2004JD005536.

Holton, J. R. (2004), *An Introduction to Dynamic Meteorology*, *Int. Geophys.*, vol. 88, 4th ed., Elsevier, New York.

Jiang, J. H., and D. L. Wu (2001), UARS MLS observations of gravity waves associated with the arctic winter stratospheric vortex, *Geophys. Res. Lett.*, *28*, 527–530.

Jiang, J. H., B. Wang, K. Goya, K. Hocke, S. D. Eckermann, J. Ma, D. L. Wu, and W. G. Read (2004), Geographical distribution and interseasonal variability of tropical deep convection: UARS MLS observations and analyses, *J. Geophys. Res.*, *109*, D03111, doi:10.1029/2003JD003756.

Lübken, F.-J. (1992), On the extraction of turbulent parameters from atmospheric density fluctuations, *J. Geophys. Res.*, *97*, 20,385–20,395.

Lübken, F. J. (1997), Annual variation of turbulent energy dissipation rates at high latitude as determined by in situ measurements of neutral density fluctuations, *J. Geophys. Res.*, *102*, 13,441–13,456.

Phillips, O. M. (1967), The generation of clear-air turbulence by the degradation of internal waves, in *Atmospheric Turbulence and Radio Wave Propagation*, edited by A. M. Yaglom and V. I. Tatarsky, pp. 130–136, Nauka, Moscow.

Sica, R. J., and A. T. Russell (1999), How many waves are in the gravity wave spectrum?, *Geophys. Res. Lett.*, *26*, 3617–3620.

Sofieva, V. F., et al. (2007a), Global analysis of scintillation variance: Indication of gravity wave breaking in the polar winter upper stratosphere, *Geophys. Res. Lett.*, *34*, L03812, doi:10.1029/2006GL028132.

Sofieva, V. F., A. S. Gurvich, F. Dalaudier, and V. Kan (2007b), Reconstruction of internal gravity wave and turbulence parameters in the stratosphere using GOMOS scintillation measurements, *J. Geophys. Res.*, *112*, D12113, doi:10.1029/2006JD007483.

Staquet, C., and J. Sommeria (2002), Internal gravity waves: From instabilities to turbulence, *Annu. Rev. Fluid Mech.*, *34*, 559–593.

Tatarskii, V. I. (1971), *The Effects of the Turbulent Atmosphere on Wave Propagation*, 417 pp., U. S. Dep. of Commer., Springfield, Va.

Whiteway, J. A., and A. I. Carswell (1995), Lidar observations of gravity wave activity in the upper stratosphere over Toronto, *J. Geophys. Res.*, *100*, 14,113–14,124.

Wilson, R., M.-L. Chanin, and A. Hauchecorne (1991), Gravity waves in the middle atmosphere observed by Rayleigh lidar: 2. Climatology, *J. Geophys. Res.*, *96*, 5169–5183.

Wu, D. L., and J. W. Waters (1996), Satellite observations of atmospheric variances: A possible indication of gravity waves, *Geophys. Res. Lett.*, *23*, 3631–3634.

Zink, F., R. A. Vincent, E. Murphy, and O. Cote (2004), Comparison of radar and in situ measurements of atmospheric turbulence, *J. Geophys. Res.*, *109*, D11108, doi:10.1029/2003JD003991.

F. Dalaudier, Service d'Aeronomie du CNRS, F-91371 Verrières-le-Buisson Cedex, France.

A. S. Gurvich, A. M. Oboukhov Institute of Atmospheric Physics, Pyzhevsky 3, Moscow, 119017, Russia.

V. F. Sofieva, Earth Observation, Finnish Meteorological Institute, P.O. Box 503, Helsinki, FIN-00101, Finland.